

# Crystallographic orientation inhomogeneity and crystal splitting in biogenic calcite

Antonio G. Checa,<sup>1,\*</sup> Jan T. Bonarski<sup>2</sup>, Marc G. Willinger<sup>3</sup>, Marek Faryna<sup>2</sup>, Katarzyna Berent<sup>2</sup>,  
Bogusz Kania<sup>2</sup>, Alicia González-Segura<sup>4</sup>, Carlos M. Pina<sup>5</sup>, Jan Pospiech<sup>2</sup> and Adam Morawiec<sup>2</sup>

<sup>1</sup> *Departamento de Estratigrafía y Paleontología, Facultad de Ciencias, Universidad de  
Granada, Granada, Spain*

<sup>2</sup> *Institute of Metallurgy and Materials Science of the Polish Academy of Sciences, Kraków,  
Poland*

<sup>3</sup> *Department of Inorganic Chemistry, Fritz Haber Institute of the Max Planck Society, Berlin,  
Germany*

<sup>4</sup> *Centro de Instrumentación Científica, Universidad de Granada, Granada, Spain*

<sup>5</sup> *Departamento de Cristalografía y Mineralogía, Facultad de Ciencias Geológicas, Universidad  
Complutense de Madrid, Madrid, Spain*

-----

\* Corresponding author. Tel.: + 34 958243201; fax: + 34 958248528.

E-mail address: [acheca@ugr.es](mailto:acheca@ugr.es)

Postal address: Departamento de Estratigrafía y Paleontología, Facultad de Ciencias,  
Universidad de Granada, Avenida Fuentenueva s/n, 18071-Granada, Spain

URL: <http://www.ugr.es/~estratig/>

The calcitic prismatic units forming the outer shell of the bivalve *Pinctada margaritifera* have been analysed using SEM-EBSD, TEM and AFM. In the initial stages of growth, the individual prismatic units are single crystals. Their crystalline orientation is not consistent but rather changes gradually during growth. The gradients in crystallographic orientation occur mainly in a direction parallel to the long axis of the prism, i.e. perpendicular to the shell surface and do not show preferential tilting along any of the calcite lattice axes. At a certain growth stage, gradients begin to spread and diverge, implying that the prismatic units split into several crystalline domains. In this way, a branched crystal, in which the ends of the branches are independent crystalline domains, is formed. At the nanometer scale, the material is composed of slightly misoriented domains, which are separated by planes approximately perpendicular to the *c*-axis. Orientational gradients and splitting processes are described in biocrystals for the first time and are undoubtedly related to the high content of intracrystalline organic molecules, although the way in which these act to induce the observed crystalline patterns is a matter of future research.

Keywords: Crystallography; biomineralization; bivalves; calcite; EBSD

Running title: Instabilities in biocrystals

## 1. INTRODUCTION

The knowledge of the crystallography of biocrystals is an essential topic in order to understand their structure, initiation and mode of growth. Within invertebrates, molluscs are unrivalled masters in the formation of crystalline calcium carbonates, taking into account the big array of crystal shapes and distributions (i.e. the so-called microstructures) which they are able to produce. The crystallography of biominerals formed by molluscs has been investigated using several techniques, including high-resolution synchrotron X-ray diffraction (XRD) (e.g., [1]), X-ray photoelectron emission spectromicroscopy (X-PEEM) [2] and electron back-scatter diffraction (EBSD) [3]. According to these studies, biocrystals diffract (X-rays, electrons, etc) in a similar way to single crystals on the meso-scale. Some authors have shown that some microstructural units may be polycrystalline. The use of etching protocols has demonstrated that nacre tablets of gastropods are composed of domains (sometimes several tens of domains), corresponding to single crystals twinned on {110} planes [4]. The dome-shaped crystals of aragonite, which initiate the nacre of *Pinctada*, have been shown by TEM to consist of a complex arrangement of crystalline domains with diverse orientations [5]. The columnar calcitic prismatic units forming the outer layer of *Pinctada* consist of several subunits [6,7] each, with complex boundaries, which were shown by TEM-EBSD to display a considerable degree of mutual misorientation [8]. These same units were shown to display large variations in the orientations of their *c*-axes [9], hence being different crystallographic domains. Intraprismatic domains are much longer than wide because they extend parallel to the long axis of the main prismatic unit with growth. Although there is a considerable range of sizes, they should rather be considered as microstructural units.

Biocrystals are known to display an internal ultrastructure, composed of submicron-sized particles. This is referred to as mesocrystalline behaviour [10]. Previous authors [1,11], using high-resolution synchrotron XRD, determined coherent domains with lengths ranging from 300 to 750 nm for the calcitic prisms of two species of *Atrina* and one of *Pinna*, with very low mosaicity ( $0.03^\circ$  for *A. serrata* [1], and  $<1^\circ$  for *P. nobilis* [12]). They are anisotropic in shape, extending differently along diverse crystallographic directions [11]. These findings are in good agreement with the TEM observations [8,13] of intracrystalline sub-micron partitions with different diffraction contrasts, which were limited by discontinuously aligned biomacromolecules. Up to now, no data on the misorientation between adjacent nanodomains have been provided, although values  $< 2^\circ$  can be inferred from figure 2 in Okumura *et al.* [8].

The nanostructure of biocrystals has also been investigated with atomic force microscopy (AFM). Dauphin [14] was the first to observe that the nacre of cephalopods was composed of irregular amalgamated granules of diameters between 40 and 50 nm. Furthermore, AFM- and scanning electron microscopy (SEM)-based work has revealed that such nanostructures are common to carbonate biocrystals secreted by sponges [15], corals [16], molluscs [17] and echinoderms [18]. The component granules in all these materials range in size from 30 to 200 nm; therefore, these morphological nanodomains are much smaller than the ones revealed by TEM.

The columnar prismatic microstructure forming the outer shell layer of many pteriomorphs bivalves (pearl oysters, fan mussels, oysters, scallops and others) is the most intensively studied calcitic biomaterial secreted by molluscs, being second only to iconic nacre, if the aragonitic microstructures are also included. In order to increase the level of completeness and resolution of the crystallography of such material with respect to previous studies [8,9], a complete EBSD

study of the calcitic columnar prisms of the outer shell layer of the black-lipped pearl oyster *Pinctada margaritifera* has been performed. The crystallographic data obtained with EBSD have been checked with TEM and AFM. Our study shows that the EBSD orientation patterns are unexpectedly unlike those of abiogenic crystals. In this paper, we will describe the results of our study and discuss their implications.

## 2. MATERIAL AND METHODS

### 2.1. Material

Specimens of the bivalve *Pinctada margaritifera*, from French Polynesia, were purchased from Conchology Inc. Specimens of the bivalve *Pinna nobilis* (off Almería, SE Spain; collection of the Departamento de Estratigrafía y Paleontología of the Universidad de Granada, EPUGR), which also has a similar outer calcitic columnar prismatic layer, were also used. In all cases, the specimens were taken live and the shells cleaned and stored under dry conditions. For comparison, two samples of geological calcite were also studied. One of them was a speleothemic calcite from Sierra de Baza (Spain). The other was a high optical grade, single crystal from Durango (México) of hydrothermal origin. Observations on a variety of species of *Pinctada* and other pteriomorphs in the collections of the EPUGR, have also been made.

### 2.2. SEM-EBSD

Samples of the outer prismatic layer of *Pinctada* and of the two geological calcites were prepared and analyzed at the Institute of Metallurgy and Materials Science (IMIM) of the Polish Academy of Sciences in Kraków. Polishing was carried out on horizontal diamond-impregnated discs (Struers DP-U2 type polisher) with grit sizes 1 and 0.25  $\mu\text{m}$ . This polishing protocol

produced maps of good image quality (figure 2a, top), as well as a high percent of adequately indexed patterns (a case of a cleaned up map is shown in figure 2a, bottom). Sections were made approximately parallel to the long axis of prisms. Nevertheless, in our maps prisms have frequently been cut obliquely. According to their elongations we have estimated that the angles of divergence of their axes from the cutting plane are between 6° and 12°. Samples were analysed using orientation imaging microscopy in low vacuum conditions in the FEI Field Emission Gun (FEG) SEM Quanta 3D microscope of the IMIM. Due to operation in low vacuum mode, no coating was necessary. A special cone was attached to the SEM pole piece to minimize the so-called "skirt effect" of the primary electron beam and reduce the gas-path length. Acceleration voltage was between 10 and 15 kV. Analysis software (TSL OIM version 5.3) was used to post-process the EBSD measurements. All data with a confidence index (CI) below 0.1 were removed. Measurements were taken at step sizes between 500 and 50 nm. For visualization purposes the following cleanup procedure was applied: 1. Grain CI standardization, 2. Neighbor orientation correlation, 3. Neighbor CI correlation.

### 2.3. TEM

Samples of the columnar calcite of the bivalve *Pinctada margaritifera* were first mechanically polished and subsequently thinned down to electron transparency with a GATAN precision ion polishing system (PIPS) at the Fritz-Haber Institute of the Max-Planck Society in Berlin. TEM analysis was carried out using the Jeol 2200FS microscope at the University of Aveiro, Portugal. For the Scanning TEM (STEM) observations we used high-angle annular dark field (HAADF). We chose the imaging conditions so as to have also diffraction contrast in our images (by selecting a relatively large camera length); in this way, the detector acts basically as an Annular

Dark Field detector, which is sensitive to changes in crystallographic orientations and scattering of the imaged object.

#### 2.4. AFM

For AFM observations, a sample of the shell of *Pinctada margaritifera* was polished, through a protocol adapted from Nouet *et al.* [19]. We used Struers water-grinding papers (DP Mol and DP Dur), followed by a thin polishing with Struers diamond pastes (3, 1, and 0.25  $\mu\text{m}$ ) and finally silica gel suspension ( $\sim 3$  h). The sample was etched in a 0.1% wt. acetic acid with 3% glutaraldehyde solution for 8 s. It was later repolished, immersed in commercial bleach for  $\sim 90$  seconds and dried before placing in the AFM sample holder. Observations were made in air using an AFM (Multimode Veeco) of the Centro Nacional de Microscopía Electrónica (Universidad Complutense de Madrid). AFM images were recorded in Tapping Mode<sup>TM</sup> while displaying cantilever height, phase and amplitude signals. Recorded AFM images were subsequently analysed using the Nanoscope 5.30r3sr3 and Nanotec WSxM. 2.1 softwares [20].

#### 2.5 FESEM

Additional observations on the shells of several species of *Pinctada* and other Pterioidea and Pinnoidea have been made with the Field Emission SEM (FESEM) Zeiss Leo Gemini of the Centro de Instrumentación Científica of the Universidad de Granada.

### 3. RESULTS

#### 3.1. SEM-EBSD

*Pinctada* has an outer layer with calcitic columnar prismatic microstructure, which is underlain by a nacre layer. This microstructural arrangement is common to the rest of the pterioid bivalves (the group which includes the pterioideans or pearl oysters, and the pinnoideans, or fan mussels). The calcitic layer consists of large prismatic units (up to several hundred microns long) which elongate in perpendicular to the shell's outer surface, i.e. in the growth direction of the prisms (figures 1, 2*a,b*, and 3*a*). As usual, many units tend to disappear towards the shell interior at the same time as the surviving units expand in width (figure 1). Units (called here first-order units; FOU) are surrounded by micrometric organic walls (figure 1). In the case of *Pinctada*, each FOU is usually subdivided into second-order units (SOUs) [6,7,8,9] (see figures 2*a,b*, 3*a* and 4*a*).

Orientation maps reveal that FOU as well as SOUs characteristically display colour gradients which propagate in both the vertical (i.e. growth) and horizontal directions, (figures 2*a,b*, 3*a*, 4*a* and 5). Angular misorientation along these gradients can be very high, particularly in parallel to the long axis of the prisms (in some instances, we have measured values above 40°; figure 2*c*, and table S1). Some misorientation profiles perpendicular to the growth direction of the FOU, display repeated oscillations (figure 2*c*, profiles 1, 2 and 6).

After a certain shell thickness has been secreted, distinct demarcation lines, which separate areas with increasingly different orientations, begin to appear along some FOU (figures 2*b*, 3*a* and 5*b*). Misorientation profiles show a distinct change across these lines, so that the change is no longer gradual, but abrupt (figure 2*c*, profiles 2, 3 and 5). This implies that, at these positions, the initial crystal splits and transforms into two or more sub-grain crystalline domains. Splitting becomes more intense towards the shell interior, i.e. the number of new branches (crystalline domains) increases towards the shell interior (figures 2*b* and 3*a*). We have often recorded

divergences between SOUs in the orientation of the *c*-axis of  $\sim 20^\circ$ , while Gilbert *et al.* [9] found values of up to  $50^\circ$ . At some growth interruptions (evidenced by marked growth lines enriched in organic matter) the calcitic crystals may emerge *de novo*, (rarely) cease to grow, or shift their positions (figures 2*a,b*, and 3*a*).

The identified boundaries between SOUs are complex, locally dendritic and, sometimes, areas belonging to a given crystal can become totally isolated within the neighbouring crystal (figures 3*a* and 4*a*), although we cannot rule out connections in the third dimension.

For particular crystals the inverse pole figures (IPFs) indicate that the pole paths do not take any defined trend (figures 3*b* and 5). For example, in the case depicted in figure 5*a* the path is oscillating, with the pole maximum shifting, first to the left and then to the right. The recorded trends do not follow radii subtending from any of the corners of the IPF (figure 5*a*), but are rather oblique, implying that the calcite lattice rotates around a changing axis which does not coincide with either the *c*- or the *a*-axes (figures 3*b* and 5*a*). The same patterns are observed for those FOU's which split with growth, with the difference that the splitting process is evident upon examination of the IPF maxima, which progressively broaden and branch into several independent growth trajectories (figure 5*b*).

In the different transects, most misalignment values are above the experimental error ( $0.5^\circ$ ), with some values rising above  $3^\circ$  (figure 2*c*, and table S1). Above this value, splitting typically takes place. The boundaries between SOUs become clearly delineated for point-to-point misorientations  $\geq 4^\circ$  (figure 4*b*).

The orientation maps made on *Pinna nobilis* show that, within each prismatic unit, there are no changes in color, implying absence of orientation gradients and splitting events (figure S1*a*). Misorientation profiles reveal point-to-point misorientation values similar to those

recorded in *Pinctada margaritifera*, but point-to-origin profiles do not show appreciable trends (figure S1*b,c*, and table S1).

The orientation maps acquired from the speleothemic calcite from Baza show that each crystal displays a uniform internal orientation, without having any evidence of orientational gradients (figure S2*a,b*). This is also revealed by both the small spread of the IPF maxima (figure S2*c*) and by the misorientation profiles across particular crystals, which do not show any recognisable trend (figure S2*d*, and table S1). The point-to-point misorientation data are within the range of those found in biogenic calcite (table S1). The colour maps for the hydrothermal calcite from Durango (figure S1*e*) are even more homogeneous than those of the speleothemic calcite, which fits in with both the extremely reduced pole maxima (figure S1*f*) and the average point-to-point misorientation (figure S1*g*, and table S1), well below the experimental error. This is most probably the result of the high degree of crystallinity of the material.

### 3.2. TEM

TEM revealed areas within FOU's which show very different diffraction contrast (i.e. electron diffraction in the crystalline material depends on the orientation with respect to the electron beam) (figure 6*a-c*) which is caused by local variations of the crystallographic orientation. Figure 6*d* shows a case in which the variation in the orientation of the *c*-axis, based on lattice fringes, measured around 4°. The sharp contrast change between the lower and upper parts in figure 6*d* also indicates a slight rotation around the *a*-axis. The boundaries between different crystalline domains are irregular and slightly dendritic (figure 6*a-c,e*). Occasionally, the formation of peninsulas and islands of domains within a differently oriented matrix can be discerned by the difference in diffraction contrast in bright field images (figure 6*a-c,e-g*). They clearly correspond

to the different SOUs identified during SEM and EBSD analysis. Both, the jagged aspect of the boundaries as well as the existence of some units, isolated or semi-isolated within areas of different contrast, imply that the SOUs recognized with TEM have a substructure of polygonal units.

This observed nanostructure is also evident from observations within areas of similar diffraction contrast, which reveal that the ultrastructure consists of a network of polygons with different contrast (figure 6*h,i*). Their boundaries are jagged and irregular, although they follow a predominant direction, which is shown by selected area diffraction to be perpendicular to the *c*-axis (figure 6*i*). These boundaries are crossed by other boundaries at different angles (mostly perpendicular or at a high angle). Together, they delineate a pattern of irregular parallelogram-like units of calcite. Their sizes vary, but are within the range of 200x500 nm. The subtle differences in contrast between the nanodomains imply small misorientation values.

### 3.3. AFM

AFM images of polished cross sections of *Pinctada margaritifera* reveal the nanounits that form the calcitic prisms (figure 7*a-c*). These nanounits are approximately 50-150 nm in size and they appear partially coated by a thin membrane clearly recognisable in the height and amplitude images (figure 7*d,e*). Typically, the thickness of such a membrane ranges from 0.5 to 1.5 nm (figure 7*f*). After the sample was treated with bleach for about 90 s, most of the membrane was removed from the surface and only some remains attached to the nanounits could be seen. Phase images reveal a clear contrast between the nanounits and the covering membrane, with the former appearing much brighter. Such a contrast indicates that nanounits are harder than the

membrane. All together, these observations indicate that the membranes most likely have an organic nature.

### 3.4. FESEM

On the growth surface of the prismatic crystals of *Pinctada margaritifera* (as well as in other species of the same genus), we have noticed the presence of a substructure of minor globular nanounits (30 to 80 nm in diameter) (figure 8), which might be the carbonate globules identified with AFM (figure 7). The nanounits sometimes cluster into more or less well-defined rhombohedral aggregates (Figure 8a).

## 4. DISCUSSION

Our EBSD study demonstrates that the prismatic layer of *Pinctada margaritifera* is formed by long prismatic units (first-order prismatic units, FOU) which do not have a constant crystallographic orientation. In particular, FOU are characterized by having gradients in orientation, which are more noticeable in parallel to the long axis of the unit, although they can be perpendicular or oblique to this direction (figures 2, 3 and 4).

The orientation maps (figures 2*b*, 3*a* and 4*a*) and the inverse pole figures (figures 3*b* and 5*a*) patterns also imply that poles of particular crystals do not have linear but winding and sometimes oscillating paths, which are independent from those of their neighbouring crystals. Also, the different FOU begin at the shell surface as single crystals, until at a certain growth stage they begin to split into minor crystalline units (second-order units, SOU) the intricate boundaries between them being characterized by sharp changes in misorientation (typically  $> 4^\circ$ ; figure 4*b*). Associated inverse pole figures show that splitting is manifested as a local divergence in

gradients (figure 5b). After splitting, the SOUs continue to display internal orientational gradients (figures 2b, 3a, 4a and 5b). The splitting both of FOU's and SOUs may continue with growth until the prismatic unit becomes a complex branched crystal in which the branches become progressively different crystalline domains (figures 2b, 3a and 4a). In this way, new crystallographic domains (SOUs) develop from FOU's, without the need of nucleation events.

Checa *et al.* [21] reported that the individual calcitic prisms (FOU's) of the oyster *Ostrea edulis* and of the scallop *Propeamussium dalli* (both are members of the Ostreoida, which, together with the Pterioidea, are included within the Pteriomorphia) also display longitudinal orientational gradients (figure S3). Pole figures for individual profiles (figure S3c,d) show changes in orientation both in the *c*- and *a*-axes. A re-examination of these data shows that, in addition, cases of crystal splitting, though not so marked as those recorded in *P. margaritifera*, are also frequent in the prisms of *O. edulis* (figure S3b,d).

Besides their existence in a number of bivalves with calcitic layers, we have detected gradients also in the fibrous aragonitic prisms of the bivalve *Neotrigonia* (unpublished observations). Therefore, the reported orientational gradients may be a common phenomenon in molluscan biocrystals.

TEM revealed areas within FOU's which were in very different Fresnel contrast, implying also different orientations (figure 6), and which clearly correspond to different SOUs (figure 6a-g). These areas are in turn composed of nanodomains, which have boundaries approximately perpendicular or at a relatively high angle to the *c*-axis (figure 6h,i). These nanodomains display subtle differences in contrast, which should also correspond to minor misorientations. Unfortunately, neither data from the literature nor our TEM data directly revealed the existence of dislocation lines on the material. Okumura *et al.* [13], with TEM, noted similar domains in the

prismatic calcite of several bivalves having misoriented boundaries (no quantitative data were provided). Suzuki *et al.* [22] reported similar nanograins in the calcitic spherulitic prismatic units of the outermost layer of a limpet, which also showed small misalignments. The TEM data fit in with the point-to-point misorientation values we have measured with EBSD (table S1).

The nanodomains detected with TEM (figure 6) are dissimilar in size and shape to the organic-coated globules which we observed with AFM (figure 7) and FESEM (figure 8) and which have been previously reported by other authors [14,17,23], these being irregularly rounded in shape and much smaller (30-100 nm). Both features constitute different ultrastructural levels.

The orientational gradients and splitting processes described in biocrystals are known in natural or synthetic materials subjected to deformation (e.g., [24-26]), with the difference that the former happen at surface ambient temperature and pressure. In fact the available EBSD data are qualitatively identical. A similar, process was described by García-Ruiz *et al.* [27] in the so-called witherite biomorphs, which show repeated processes of crystal splitting during growth (see also review in [28]). These authors interpreted these processes according to previous models [29], which establish that non-absorbable polymer impurities adhering at the growth front cause the formation of new crystals which are slightly misoriented with respect to the crystalline lattice. In these cases, we do not yet know if splitting also has the gradual nature we have observed in biogenic calcite. Other geological minerals growing at surface temperature show similar features, as in the case of the saddle dolomite, which is characterized by curved crystal faces resulting from misoriented microdomains, due to the superposition of growth increments in which the composition oscillates [30,31].

The existence of gradients in aragonite of biological origin (see above) allows us to rule out the effect of magnesium ions being incorporated within the crystal lattice as a possible origin of the observed orientational instabilities.

The most evident difference between biogenic and geological or synthetic materials is the presence of occluded intracrystalline biomolecules. Berman *et al.* [1], using high-resolution synchrotron X-ray radiation, found a coherence length of some 300 nm in the calcite prisms of the pinnoidean bivalve *Atrina*. They attributed this pattern to the adhesion of organic molecules to specific planes that prevent crystal growth in the perpendicular direction. Li *et al.* [32] observed with TEM tomography disk-like nanopatches in the calcite of *Atrina*, where scattering intensity is consistent with organic inclusions. These nanopatches are preferentially aligned with the (001) calcite planes. Along the crystallographic *c*-axis, there are alternating organic-rich and -poor regions on a length scale of tens of nanometers, while, in the perpendicular directions, the distribution of nanopatches is more random and uniform. Gilow *et al.* [12] also concluded that organic molecules attach preferentially to the highly charged {001} planes of the prismatic calcite of *Pinna* (which is a close relative of *Atrina*). A similar pattern has been recently observed in the nacre of the mussel *Perna* [33]. Organic molecules occluded within the crystals and distributed around the boundaries of 200-300 nm crystalline domains (similar to the ones which we report here; figure 6*a-c,e-i*) were imaged with TEM in the calcites of the pterioidean *Pinctada* and in the ostreoidean *Crassostrea* [13,34]; the boundaries are characterized by small misorientations, in coincidence with small distortions of the crystal lattice. The same authors failed to find such patterns of misoriented domains in the calcite of the pinnoidean *Atrina*. These data strikingly match our EBSD results, which imply the existence of misorientations in *Pinctada* (figures 2*b,c*, 3*a* and 4*a*), and in *Ostrea* (same bivalve family as *Crassostrea*; figure

S3) but not in *Pinna* (same family as *Atrina*; figure S1). Although additional evidence is needed, there appears to be a correlation between the patterning into diffraction contrast nanodomains, as revealed by TEM, and misorientation trends, measured by EBSD. Okumura *et al.* [13], making TGA curves for several calcitic biocrystals, found no significant differences in the intracrystalline content of organic molecules between the prismatic calcites of *Pinctada*, *Crassostrea* and *Atrina*, which casts some doubt on the intracrystalline content as directly responsible for the misorientations measured, by means of dislocations.

Dislocations are not the only effects induced by occluded biomolecules. Pokroy *et al.* [35,36] revealed that in biological calcite and aragonite the crystal lattices are anisotropically distorted, attributing this to the action of intracrystalline biomolecules. Okumura *et al.* [13] reported significant differences in their calculated variances of lattice spacing, the values for *Pinctada* and *Crassostrea* being well above that for *Atrina*. This certainly correlates with the gradients and crystal-splitting processes recorded with EBSD in *Pinctada* and *Ostrea*, and with their absence in *Pinna* (see paragraph above). Deformation of the crystal lattice can be easily accommodated without changes in orientation (lattice rotations), but the fact that this deformation is inhomogeneous across the crystal could potentially cause intracrystalline strains, which could be resolved as long-range misorientations and, ultimately, crystal splitting, of the kind we have observed. Further work, including a large set of samples, is needed to test this hypothesis.

The nanostructure observed with AFM (figure 7) consists of granules coated with extremely thin organic pellicles. The contribution of this low-weight molecular component to the reported instability of the orientations is also a matter of investigation.

## 5. CONCLUSIONS

Our SEM-EBSD study of the calcitic prismatic outer shell layer of the bivalve *Pinctada margaritifera* has revealed two important features: (1) the crystallographic orientation within individual crystals is not constant, but fluctuates in the form of longitudinal or transversal gradients, and (2) after an initial single-crystal growth stage, the prismatic units spontaneously split into progressively different crystallographic domains. Each new crystallographic domain thus formed also develops its own orientational gradients. This behaviour is in good agreement with the nanostructural arrangement observed by TEM, consisting of slightly misoriented parallelogram-like nanodomains. It is still to be determined whether dislocation lines exist between the nanodomains as well as whether misorientations occur exactly at the boundaries between the TEM-observed nanodomains.

Although the existence of intracrystalline misorientations had been incipiently anticipated by Okumura *et al.* [8], our study provides the first clear picture of how they are distributed into orientational gradients and the first cogent explanation of the associated processes of splitting in biocrystals. This opens the window for potential biomimetic studies aimed at obtaining synthetic materials with particular crystallographic properties by simply varying the contents and types of absorbable biomolecules.

We thank Achim Klein (Fritz-Haber Institut, Berlin) for TEM sample preparation. A.G.C., A.G.-S. and C.M.P. received funding from projects CGL2010-20748-CO2-01, of the Spanish Ministerio de Ciencia e Innovación, and RNM6433 of the Andalusian Consejería de Innovación Ciencia y Tecnología, as well as the the European COST Action TD0903. M.-G. W was funded by FCT projects PTDC/CTM/100468/2008 and REDE/1509/RME/2005 of the Portuguese Ministério da Educação e Ciência. A.G.S. and C.M.P. also acknowledge the Centro de

Instrumentación Científica (Univ. Granada) and the Centro Nacional de Microscopía Electrónica (Univ. Complutense Madrid), respectively, for the use of the equipments.

## REFERENCES

1. Berman, A., Hanson, J., Leiserowitz, L., Koetzle, T. F., Weiner, S. & Addadi, L. 1993 Biological control of crystal texture: A widespread strategy for adapting crystal properties to function. *Science* **259**, 776-779. (doi:DOI:10.1126/science.259.5096.776)
2. Gilbert, P. U. P. A., Metzler, R. A., Zhou, D., Scholl, A., Doran, A., Young, A., Kunz, M., Tamura, N. & Coppersmith, S. N. 2008 Gradual ordering in red abalone nacre. *J. Am. Chem. Soc.* **130**, 17519–17527. (doi:10.1021/ja8065495)
3. Dalbeck, P., England, J., Cusack, M., Lee, M. R. & Fallick, A. E. 2006 Crystallography (electron backscatter diffraction) and chemistry (electron probe microanalysis) of the avian eggshell. *Eur. J. Mineral.* **18**, 601-609. (doi: 10.1021/cg068008t)
4. Mutvei, H. 1978 Ultrastructural characteristics of the nacre in some gastropods. *Zool. Scripta* **7**, 287–296. (doi:10.1111/j.1463-6409.1978.tb00612.x)
5. Saruwatari, K., Matsui, T., Mukai, H., Nagasawa, H. & Kogure, T. 2009 Nucleation and growth of aragonite crystals at the growth front of nacles in pearl oyster, *Pinctada fucata*. *Biomaterials* **30**, 3028-3034. (doi:10.1016/j.biomaterials.2009.03.011)
6. Dauphin, Y. 2003 Soluble organic matrices of the calcitic prismatic shell layers of two pteriomorphid bivalves *Pinna nobilis* and *Pinctada margaritifera*. *J. Biol. Chem.* **17**, 15168-15177. (doi:10.1074/jbc.M204375200)

7. Dauphin, Y., Cuif, J. P., Doucet, J., Salomé, M., Susini, J. & Williams, C. T. 2003 In situ chemical speciation of sulfur in calcitic biominerals and the simple prism concept. *J. Struct. Biol.* **142**, 272-280. (doi:10.1016/S1047-8477(03)00054-6)
8. Okumura, T., Suzuki, M., Nagasawa, H. & Kogure, T. 2010 Characteristics of biogenic calcite in the prismatic layer of a pearl oyster, *Pinctada fucata*. *Micron* **41**, 821-826. (doi:10.1016/j.micron.2010.05.004)
9. Gilbert, P. U. P. A., Young, A. & Coppersmith, S. N. 2011 Measurement of c-axis angular orientation in calcite (CaCO<sub>3</sub>) nanocrystals using X-ray absorption spectroscopy. *Proc. Natl. Acad. Sci. USA.* **108**, 11350-11355. (doi:10.1073/pnas.1107917108)
10. Cölfen, H. & Antonietti, M. 2005 Mesocrystals: Inorganic superstructures made by highly parallel crystallization and controlled alignment. *Angew. Chem. Int. Edit.* **44**, 5576–5591. (doi:10.1002/anie.200500496)
11. Pokroy, B., Fitch, A. N. & Zolotoyabko, E. 2006 The microstructure of biogenic calcite: A view by high-resolution synchrotron powder diffraction. *Adv. Mater.* **18**, 2363-2638. (doi:10.1002/adma.200600714)
12. Gilow, C., Zolotoyabko, E., Paris, O., Fratzl, P. & Barbara Aichmayer, A. 2011 Nanostructure of biogenic calcite crystals: A view by small-angle X-ray scattering. *Cryst. Growth Des.* **11**, 2054–2058. (doi: 10.1021/cg200136t)
13. Okumura, T., Suzuki, M., Nagasawa, H. & Kogure, T. 2011 Microstructural variation of biogenic calcite with intracrystalline organic macromolecules. *Cryst. Growth Des.* **12**, 224–230 (doi:10.1021/cg200947c)
14. Dauphin, Y. 2001 Nanostructures de la nacre des tests de céphalopodes actuels. *Paläont. Z.* **75**, 113-122. (doi:10.1007/BF03022601)

15. Sethmann, I., Hinrichs, R., Wöhrheide, G. & Putnis, A. 2006 Nano-cluster composite structure of calcitic sponge spicules – A case study of basic characteristics of biominerals. *J. Inorg. Biochem.* **100**, 88-96. (doi:10.1016/j.jinorgbio.2005.10.005)
16. Przeniosło, R., Stolarski, J., Mazur, M. & Brunelli, M. 2008 Hierarchically structured scleractinian coral biocrystals. *J. Struct. Biol.* **161**, 74-82. (doi:10.1016/j.jsb.2007.09.020)
17. Dauphin, Y. 2008 The nanostructural unity of mollusc shells. *Mineral. Mag.* **72**, 243-246. (doi:10.1180/minmag.2008.072.1.243)
18. Seto, J., Ma, Y., Davis, S. A., Meldrum, F., Gourrier, A., Kime, Y. Y., Schilde, W., Sztucki, M., Burghammer, M., Maltsev, S. et al. 2012 Structure-property relationships of a biological mesocrystal in the adult sea urchin spine. *Proc. Natl. Acad. Sci. USA.* **109**, 3699-3704. (doi:10.1073/pnas.1109243109)
19. Nouet, J., Baronnet, A. & Howard, L. 2012 Crystallization in organo-mineral micro-domains in the crossed-lamellar layer of *Nerita undata* (Gastropoda, Neritopsina). *Micron* **43**, 456-462. (doi:10.1016/j.micron.2011.10.027)
20. Horcas, I., Fernández, R., Gómez-Rodríguez, J. M., Colchero, J., Gómez-Herrero, J. & Baró, A. M. 2007. WSXM: a software for scanning probe microscopy and a tool for nanotechnology. *Rev. Sci. Instrum.* **78**, 013705. (doi:10.1063/1.2432410)
21. Checa, A., Esteban-Delgado, F. J., Ramírez-Rico, J. & Rodríguez-Navarro, A. B. 2009 Crystallographic reorganization of the calcitic prismatic layer of oysters. *J. Struct. Biol.* **167**, 261-270. (doi:10.1016/j.jsb.2009.06.009)
22. Suzuki, M., Kameda, J., Sasaki, T., Saruwatari, K., Nagasawa, H. & Kogure, T. 2010 Characterization of the multilayered shell of a limpet, *Lottia kogamogai* (Mollusca:

- Patellogastropoda), using SEM–EBSD and FIB–TEM techniques. *J. Struct. Biol.* **171**, 223-230. (doi:10.1016/j.jsb.2010.04.008)
23. Baronnet, A., Cuif, J. P., Dauphin, Y., Farre, B. & Nouet, J. 2008 Crystallization of biogenic Ca-carbonate within organo-mineral micro-domains. Structure of the calcite prisms of the pelecypod *Pinctada margaritifera* (Mollusca) at the submicron to nanometre ranges. *Mineral. Mag.* **72**, 617-626. (doi:10.1180/minmag.2008.072.2.617)
24. Vernooij, M. G. C., Kunze, K. & den Brok, B. 2006 ‘Brittle’ shear zones in experimentally deformed quartz single crystals. *J. Struct. Geol.* **28**, 1292-1306. (doi:10.1016/j.jsg.2006.03.018)
25. Paul, H. 2010 TEM Orientation imaging in characterization of texture changes in FCC metals. *Adv. Eng. Mater.* **12**, 1029–1036. (doi:10.1002/adem.201000078)
26. Matysiak, A. K. & Trepmann, C. A. 2012 Crystal–plastic deformation and recrystallization of peridotite controlled by the seismic cycle. *Tectonophysics* **530-531**, 111-127. (doi:10.1016/j.tecto.2011.11.029)
27. García-Ruiz, J. M., Melero-García, E. & Hyde, S. 2009 Morphogenesis of self-assembled nanocrystalline materials of barium carbonate and silica. *Science* **323**, 362-365. (doi:10.1126/science.1165349)
28. Kellermeier, M., Cölfen, H. & García-Ruiz, J. M. 2012 Silica biomorphs: Complex biomimetic hybrid materials from “sand and chalk”. *Eur. J. Inorg. Chem.* **2012**, 5123–5144. (doi:10.1002/ejic.201201029)
29. Keith, H. D. & Padden, F. J. 1963 A Phenomenological theory of spherulitic crystallization *J. Appl. Phys.* **34**, 2409-2421. (doi:10.1063/1.1702757)

30. Barber, D. J., Reeder, R. J. & Samith, D. J. 1985 A tem microstructural study of dolomite with curved faces (saddle dolomite). *Contr. Mineral. Petrol.* **91**, 82-92. (doi: 10.1007/BF00429430)
31. Searl, A. 1989 Saddle dolomite: a new view of its nature and origin. *Mineral. Mag.* **53**, 547-555.
32. Li, H., Xin, H. L., Kunitake, M. E., Keene, E. C., Muller, D. A. & Stroff, L. A. 2011 Calcite prisms from mollusk shells (*Atrina rigida*): Swisscheese-like organic–inorganic single-crystal composites. *Adv. Funct. Mater.* **21**, 2028-2034. (doi:10.1002/adfm.201002709)
33. Younis, S., Kauffmann, Y., Bloch, L. & Zolotoyabko, E. 2012 Inhomogeneity of nacre lamellae on the nanometer length scale. *Cryst. Growth Des.* **19**, 4574-4579. (doi:10.1021/cg3007734)
34. Suzuki, M., Okumura, T., Nagasawa, H. & Kogure, T. 2011 Localization of intracrystalline organic macromolecules in mollusc shells. *J. Cryst. Growth* **337**, 24-29. (doi:10.1016/j.jcrysgro.2011.10.013)
35. Pokroy, B., Quintana, J. P., Caspi, E. N., Berner, A. & Zolotoyabko, E. 2004 Anisotropic lattice distortions in biogenic aragonite. *Nature Mater.* **3**, 900-902. (doi:10.1038/nmat1263)
36. Pokroy, B., Fitch, A. N., Lee, P. N., Quintana, J. P., Caspi, E. N. & Zolotoyabko, E. 2006 Anisotropic lattice distortions in the mollusk-made aragonite: A widespread phenomenon. *J. Struct. Biol.* **153**, 145-150. (doi:10.1016/j.jsb.2005.10.009)

### Figure captions

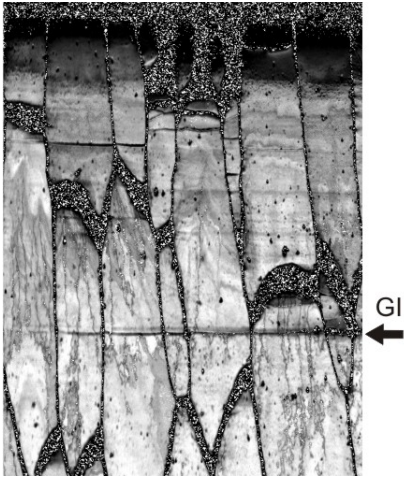


Figure 1. SEM view of a fracture of the calcitic prismatic layer of *Pinctada margaritifera*. The outer shell surface is at the top and prisms grow to the shell interior (downwards). During shell growth, many small prisms disappear, whereas the surviving units increase in size. Note organic walls surrounding prismatic units, particularly well preserved in the upper part of the layer.

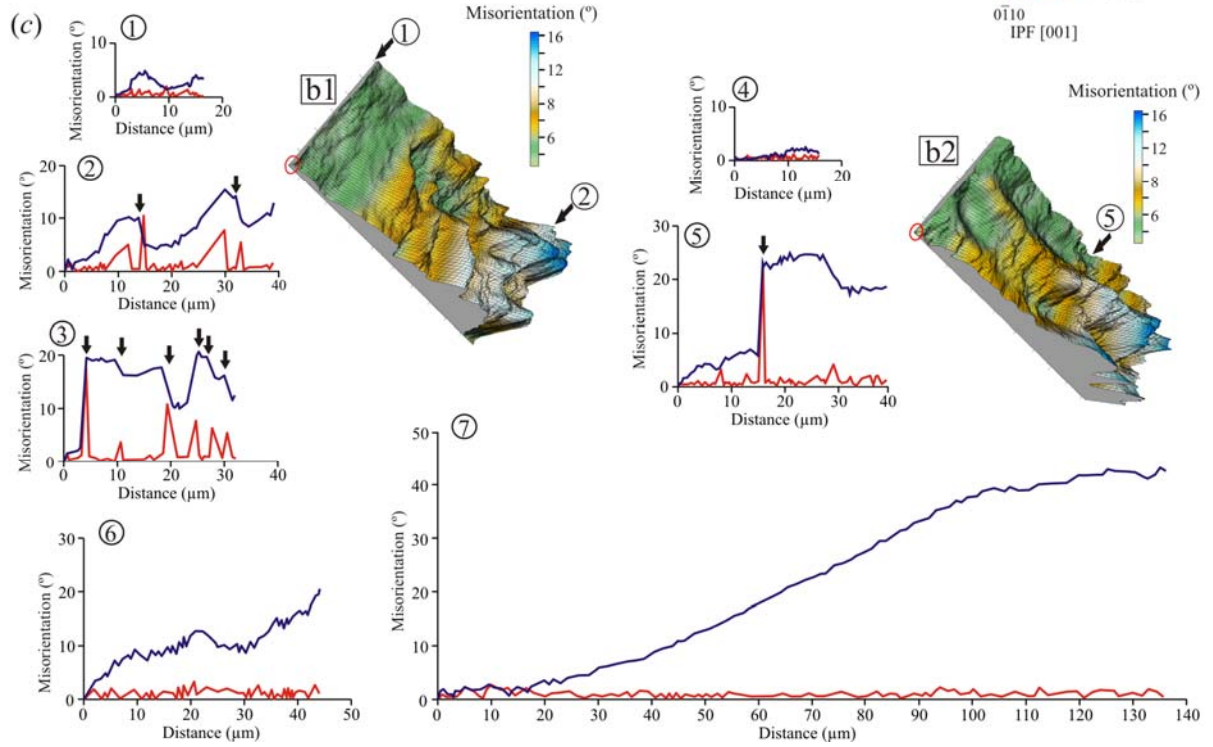
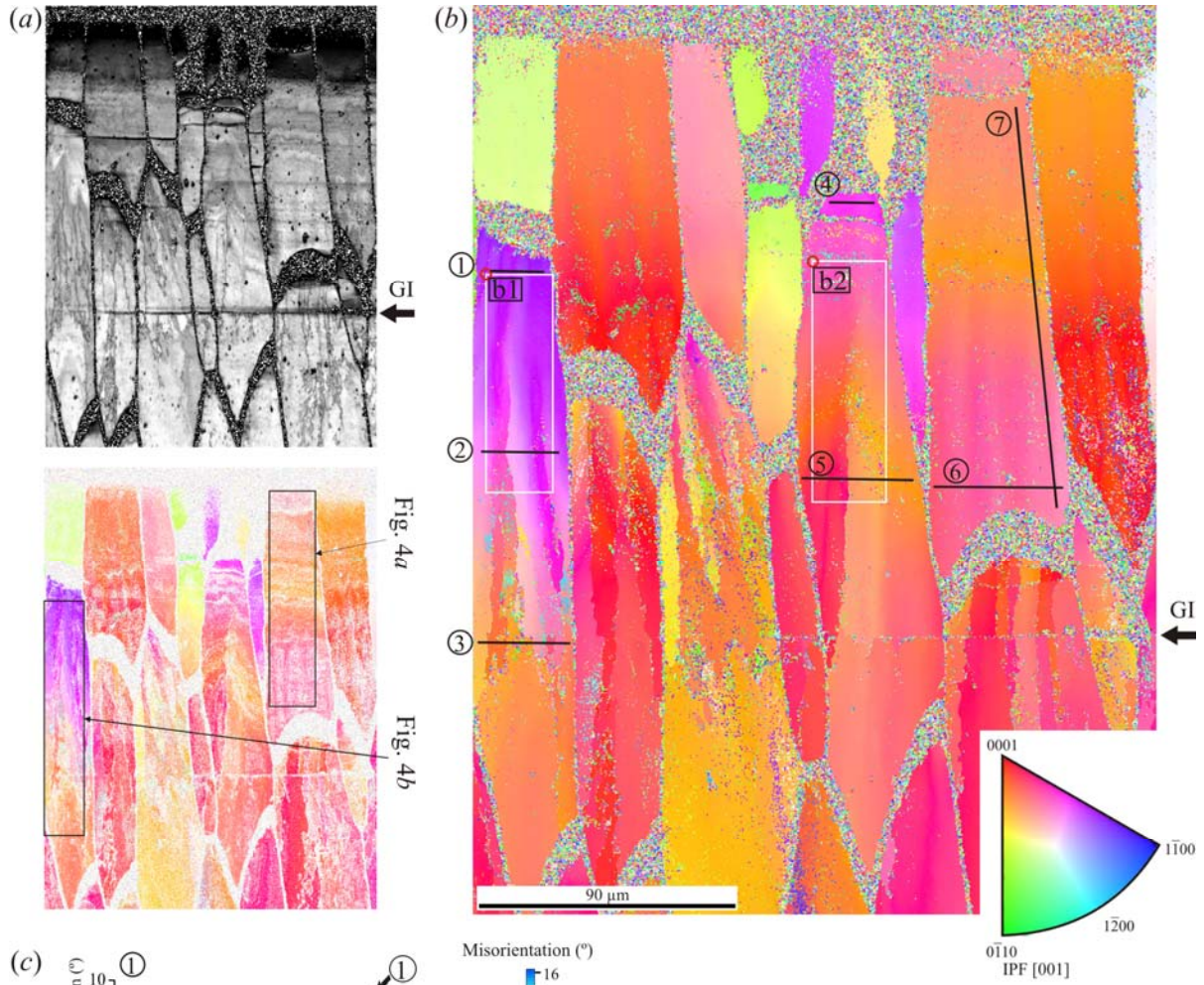


Figure 2. Orientation imaging of the outer prismatic layer of *Pinctada margaritifera*. (a) Image quality map (top) and orientation map filtered for  $CI > 0.1$  (bottom). (b) Corresponding map after clean up with reference triangle (inverse pole figure [001]; inset). (c) Misorientation profiles through the linescans 1 to 7, and 3D views of misorientation maps b1 and b2, indicated in b. Red profiles, point-to-point misorientations; blue profiles, point-to-origin misorientations. The external shell surface in a and b is at the top. GI = growth interruption. IPF = inverse pole figure.

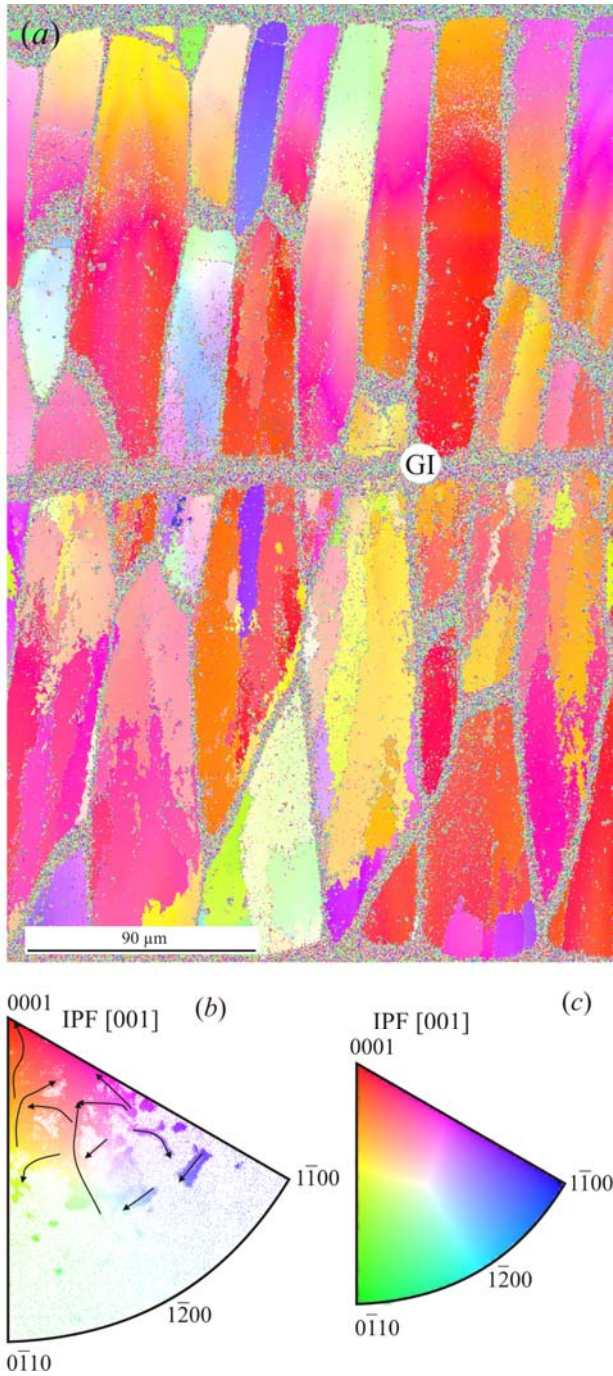


Figure 3. Orientation imaging of a cross section through the complete thickness of the calcitic prismatic layer of *Pinctada margaritifera*. The outer shell surface is to the top and the contact with the nacre is to the bottom. (a) Orientation map filtered with  $CI > 0.1$  and cleaned up. GI = growth interruption. (b) Inverse pole figure [001] of a. Note colour stripes corresponding to pole

tracks of individual crystals, some of which have been indicated with arrows. (c) Reference triangle. IPF = inverse pole figure.

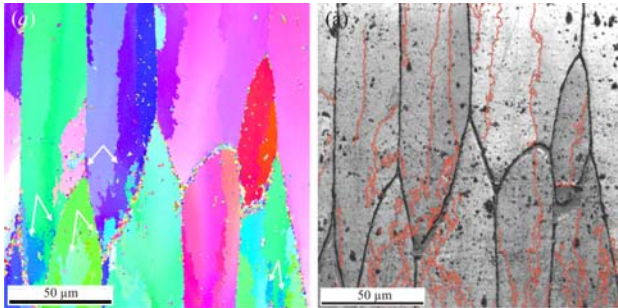


Figure 4. Orientation imaging of the calcitic layer of *Pinctada margaritifera*. (a) Orientation map filtered with  $CI > 0.1$  and cleaned up. (b) Image quality map with superimposed grain boundaries for which point-to-point misorientation is  $\geq 4^\circ$ . Double white arrows in *a* point to disconnected areas with identical orientations within single prismatic units. The growth direction of the prismatic units is to the bottom. Reference triangle as in figures 2 and 3.

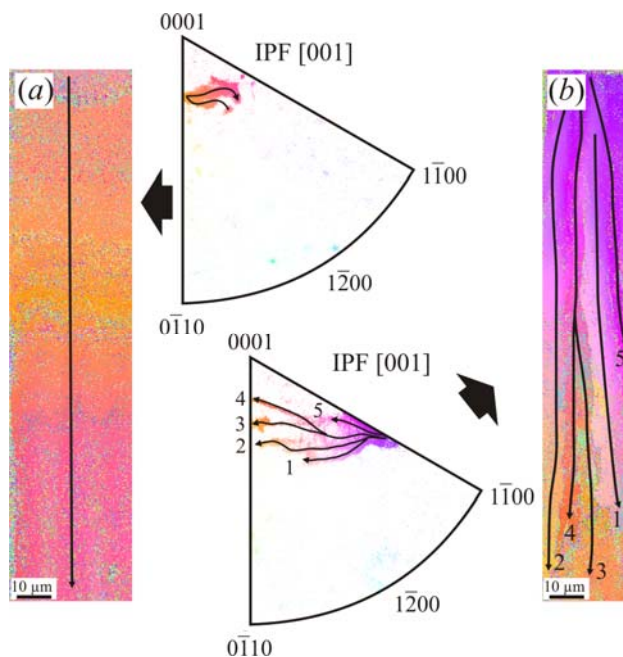


Figure 5. Orientation imaging of two selected prisms indicated in figure 1a. For each prism, the cleaned-up map (previously filtered for  $CI > 0.1$ ) and the corresponding inverse pole figure [001]

are provided. The trajectories of the poles are indicated in both the orientation map and the inverse pole figures (arrows). (a) Prism consisting of a single crystal. (b) Prism in which multiple splitting occurs at some shell depth. Note maxima oscillation in the IPF of *a* and maxima divergence and splitting in *b*. Reference triangle as in figures 2 and 3. IPF = inverse pole figure.

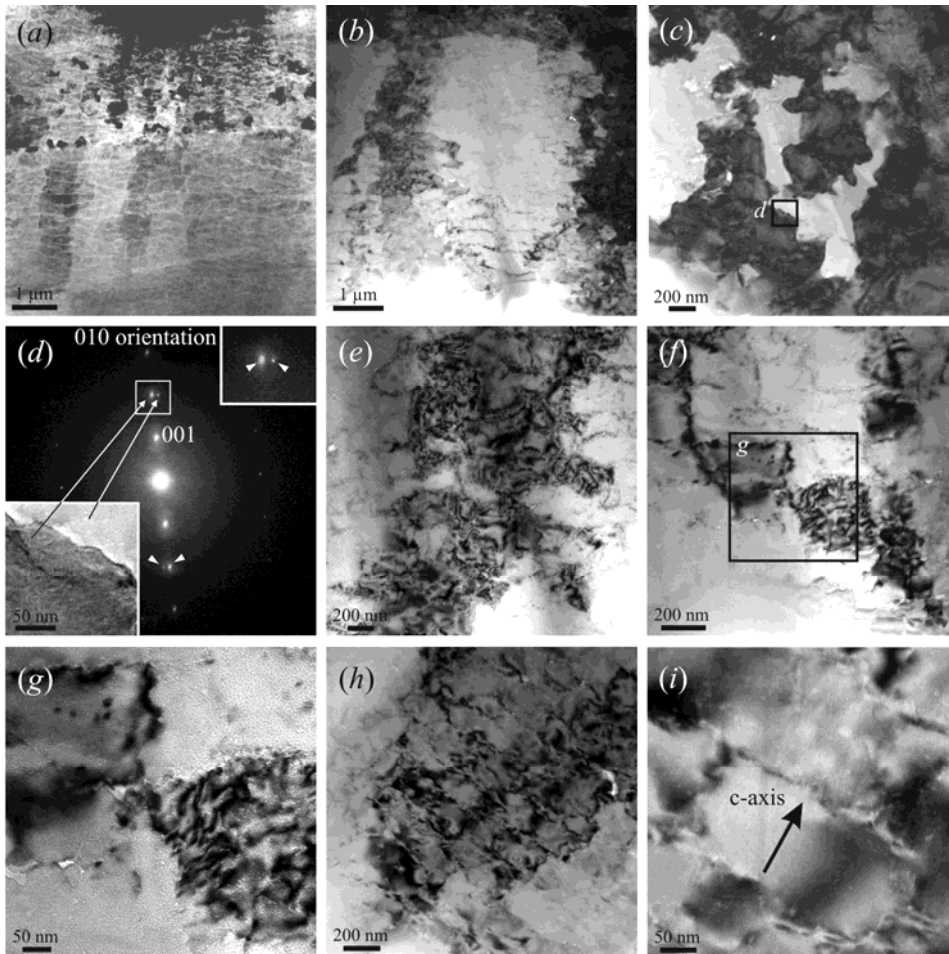


Figure 6. TEM views of the calcitic prismatic layer of *Pinctada margaritifera*. (a) General STEM view. (b,c) Progressively closer TEM views of areas with high diffraction contrast. (d) Selected area electron diffraction of the area shown in the lower left inset (framed in c). The double 001 spots (white arrows) imply that the *c*-axis rotates by  $\sim 4^\circ$  from one area to another. The upper inset is a magnification of the upper double spot (framed). (e,f,g) TEM views recorded at increasing magnifications showing areas with different diffraction contrasts and the aspect of the

nanounits composing the material. The position of  $g$  in  $f$  is indicated. ( $h,i$ ) TEM views within one region with uniform overall contrast. Note that the nanounits are delineated by thin contours of bright contrast, indicating low electron density. The orientation of the  $c$ -axis is indicated in  $i$ .

Figure 7. AFM images of a vertical polished section through the outer prismatic layer of *Pinctada margaritifera*. The images were taken in tapping mode. ( $a-c$ ) Height, phase, and amplitude images, showing the nanoblocky structure. The scale bar in  $a$  is valid for the three images. ( $d$ ) Close-up view (amplitude image) of the nanounits showing the membrane that covers the nanounits. ( $e$ ) Detail of  $d$  (position indicated). Height image. ( $f$ ) Height profile along the line p-q in  $e$ . The vertical distance between the two triangular markers (i.e. the approximate thickness of the membrane shown in  $e$ ) is 0.8 nm.

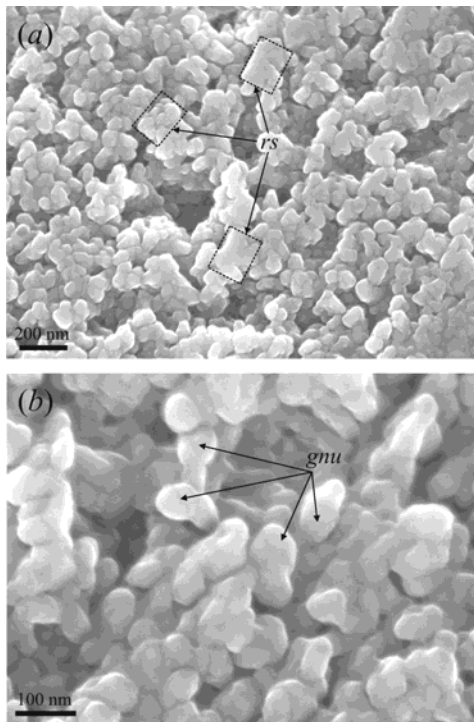
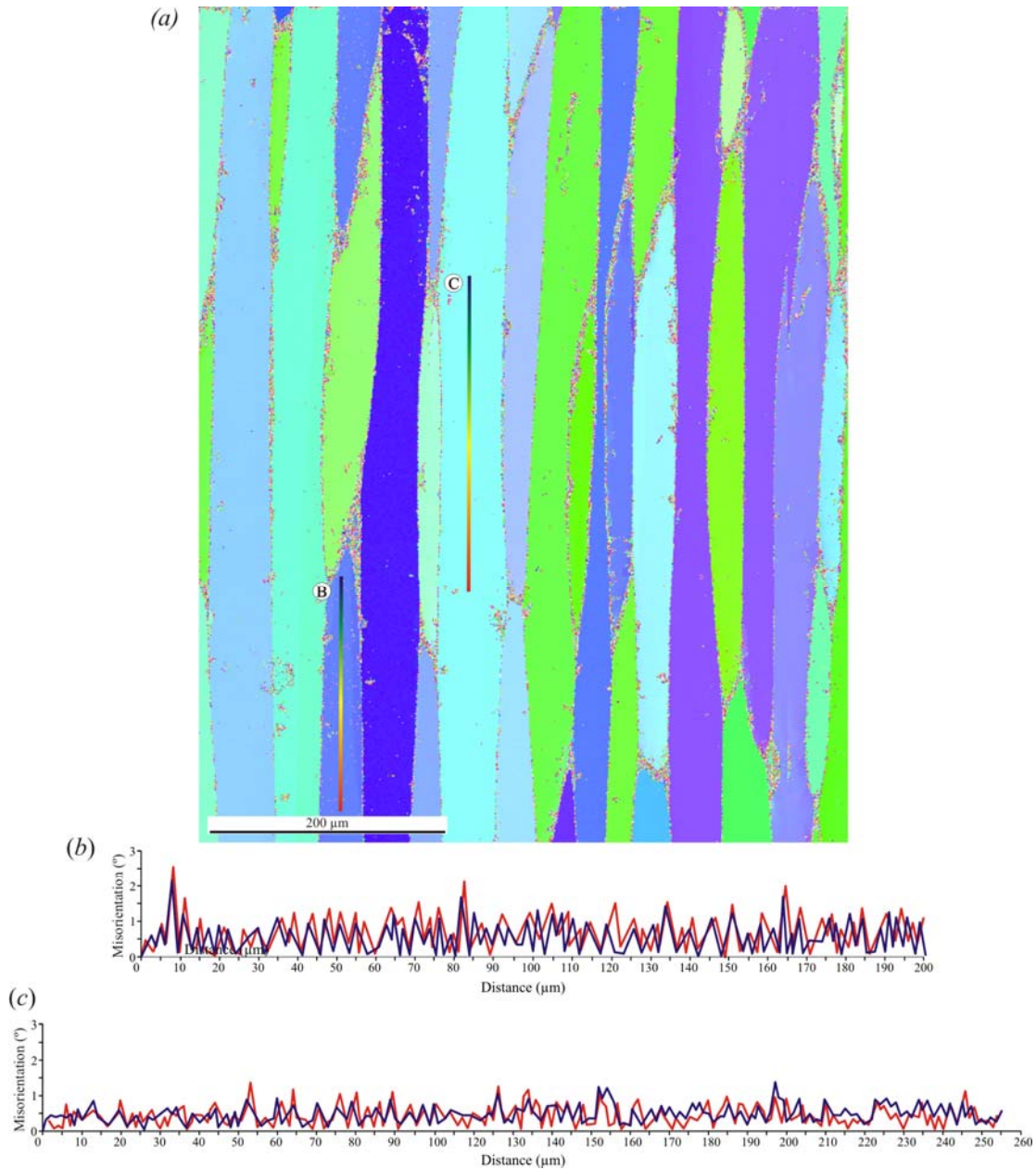


Figure 8. FESEM views of the growth surfaces of the prisms of *Pinctada margaritifera*. ( $a$ ) General view of the surface, showing the rough packing of globular nanounits into rhombohedral

subunits ( $rs$ ; indicated by rectangles). (b) Detail of  $a$ , showing the aspect of the globular nanounits ( $gnu$ ).



### Supporting Information

Figure S1. Orientation imaging of the calcitic layer of *Pinna nobilis*. (a) Orientation map filtered with  $CI > 0.1$  and cleaned up. Reference triangle as in figures 2 and 3. (b,c) Two misorientation profiles, indicated in a. Red profiles are point-to-point misorientations, whereas blue profiles are point-to-origin

misorientations.

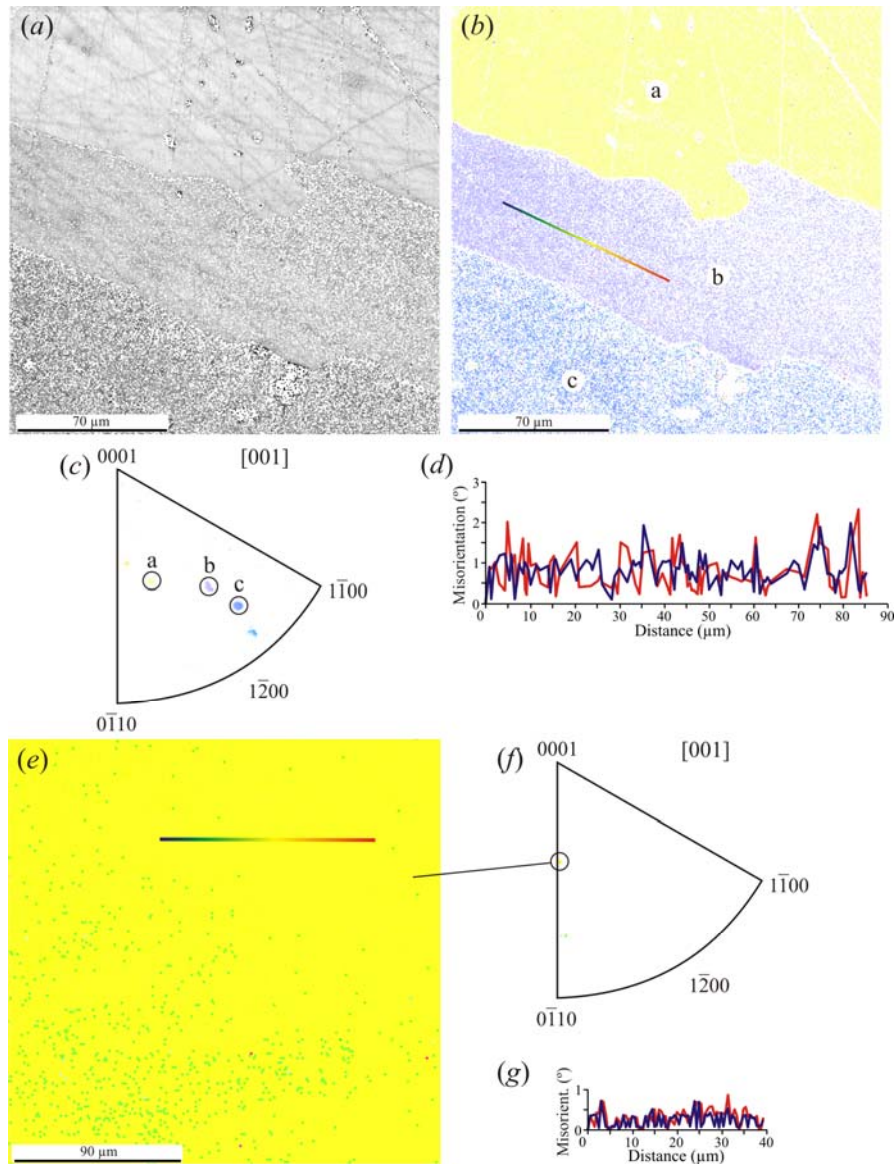


Figure S2. Orientation imaging of geological calcites. (a-d) Speleothemic calcite from Baza (Spain). (a) Image quality map. (b) Orientation map filtered with  $CI > 0.1$ . (c) Inverse pole figure [001]. (d) Misorientation profile (indicated in b). (e-g) Hydrothermal calcite from Durango (México). (e) Orientation map filtered with  $CI > 0.1$ . (f) Inverse pole figure [001]. (g) Misorientation profile (indicated in e). Red profiles in d and g are point-to-point misorientations, whereas blue profiles are point-to-origin misorientations. Reference triangle as in figures 2 and 3.

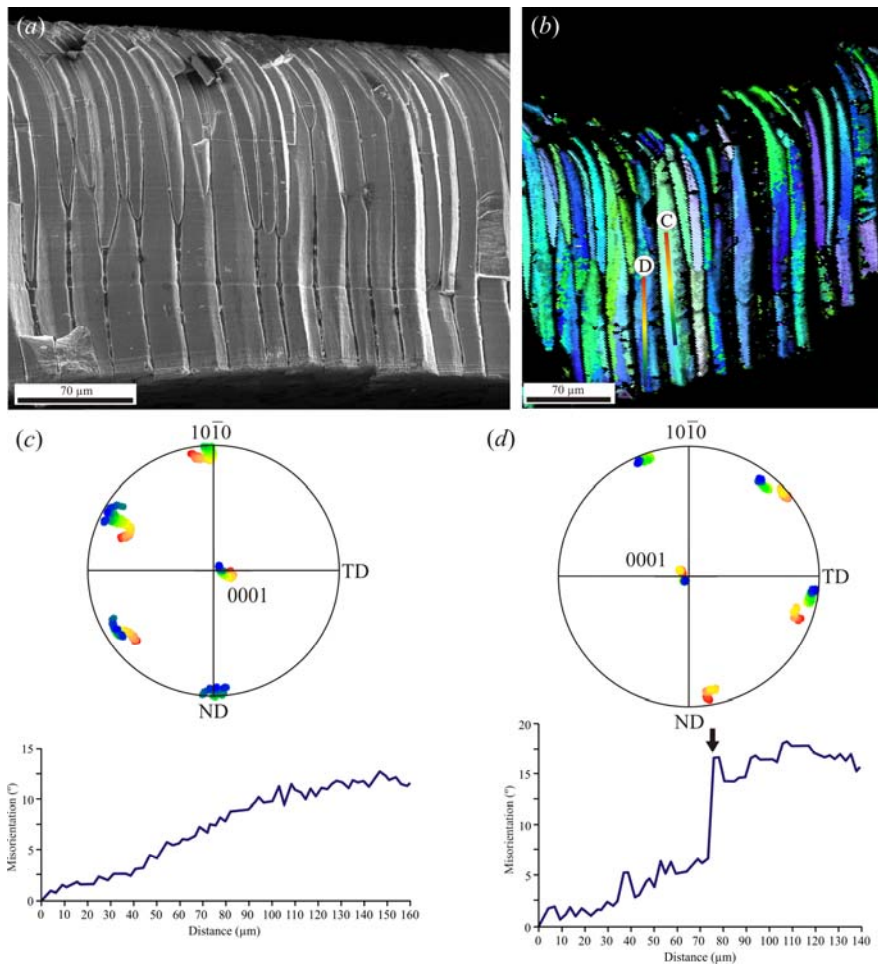


Figure S3. Orientation imaging of the calcitic layer of *Ostrea edulis*. The growth direction of the prismatic units is to the bottom. (a) SEM (secondary electron) image of the area analyzed. (b) Orientation map (reference triangle as in figures 1 and 3). (c,d) Two misorientation profiles, indicated in b. The upper graphs are the combined 0001 and  $10\bar{1}0$  pole paths and the lower graphs are the point-to-origin misorientation profiles, respectively. In the pole figures the vertical axis is the normal direction, implying that they are rotated by  $90^\circ$  with respect to the orientation map. Note step in d (indicated by an arrow), which corresponds to the transition between two SOUs within a single FOU. ND: normal direction; TD: transverse direction.

Table S1. Data for selected misorientation profiles of the materials studied.

Material/Map_profile	Mean P-P <sup>a</sup>	SD <sup>b</sup>	Max P-P <sup>c</sup>	N <sup>d</sup>	End-Or <sup>e</sup>
Pinctada margaritifera_Scan 8 (step size = 500 nm) (figure 4a)					
Profile_3	1.14	0.53	3.20	69	20.91
Profile_6	0.66	0.44	3.52	247	13.48
Pinctada margaritifera_Scan 14 (step size = 250 nm) (figure 2b)					
Profile_4 (Fig. 2c)	0.93	0.61	3.70	75	3.05
Profile_7 (Fig. 2c)	0.65	0.34	2.77	386	42.98
Profile_8	0.84	0.53	3.08	327	48.12
Profile_9	1.07	0.58	2.77	69	10.14
Pinna nobilis_Scan 3 (step size = 1 $\mu$ m) (figure S1a)					
Profile B (figure S1b)	0.84	0.50	3.03	201	0.53
Profile C(figure S1c)	0.46	0.25	1.38	245	0.58
Speleothem from Baza (step size = 500 nm) (figure S2)					
scan 1_profile 1	0.79	0.40	2.35	103	0.77
scan 4_profile 1	0.82	0.37	1.78	104	0.62
Calcite from Durango (step size = 500 nm) (figure S2)					
scan 3_profile 1 (figure S2g)	0.32	0.19	0.86	78	0.25
scan 3_profile 3	0.23	0.22	0.73	30	0.73

<sup>a</sup> Mean point-to-point misorientation. <sup>b</sup> Standard deviation. <sup>c</sup> Maximal point-to-point misorientation. <sup>d</sup> Number of data. <sup>e</sup> End-to-origin misorientation.